Quaternized Graphene Oxide Nanocomposites as Fast Hydroxide Conductors

Hadis Zarrin, Jing Fu, Gaopeng Jiang, Skylar Yoo, Jared Lenos, Michael Fowler, and Zhongwei Chen*

Department of Chemical Engineering, Waterloo Institute for Nanotechnology, Waterloo Institute for Sustainable Energy, University of Waterloo, 200 University Avenue W, Waterloo, ON Canada, N2L 3G1

ABSTRACT Nanocomposites play a key role in performance improvements of hydroxide conductors employed in a wide range of alkaline—electrochemical systems such as fuel cells and metal—air batteries. Graphene oxide (GO) nanosheets are considered to be outstanding nanofillers for polymeric nanocomposites on account of their excellent physicochemical strength and electrochemical properties. In this work, a fast hydroxide conductor was developed on the basis of a chemically modified GO nanocomposite membrane. The high surface area of GO was functionalized with highly stable hydroxide-conductive groups using a dimethyloctadecyl [3-(trimethoxysilyl)propyl]ammonium chloride (DMAOP) precursor, named QAFGO, and then composed with porous polybenzimidazole PBI (pPBI) as a well-suited polymeric backbone. The nanocomposite exhibited outstanding hydroxide conductivity of 0.085 S cm^{-1}, high physicochemical strength, and electrochemical stability for 21 days. An alkaline fuel cell (AFC) setup was fabricated to determine the functionality of QAFGO/pPBI nanocomposite in an alkaline-based system. The high AFC performance with peak power density of 86.68 mW cm^{-2} demonstrated that QAFGO/pPBI nanocomposite membrane has promising potential to be employed as a reliable hydroxide conductor for electrochemical systems working in alkaline conditions.

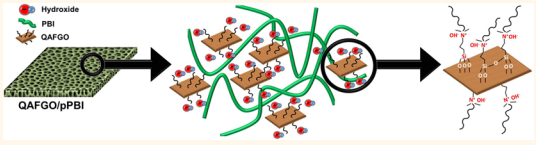

KEYWORDS: graphene oxide · nanocomposites · hydroxide-exchange membrane · ionic conductivity · alkaline fuel cells

Development of a well-designed, genuinely engineered, and fast hydroxide conductor with excellent durability is vitally required for a wide range of alkaline—electrochemical systems such as fuel cells, metal—air batteries, supercapacitors, and electrolyzers.[1] So far, different categories of homogeneous and heterogeneous hydroxide conductors[2] including (i) chemically/physically functionalized polymers,[3,4] (ii) ion-solvating polymers (ISP),[5,6] (iii) inorganic—organic composites,[7−9] and (iv) blended polymers[10] have been studied by different research groups. However, the dilemma between high hydroxide conductivity and physicochemical stability remains as an important issue; *i.e.*, maximizing one will minimize the other. Among various classifications of hydroxide conductors, inorganic—organic nanocomposites are capable of providing high hydroxide conductivity and physicochemical stability together in which nanosized fillers such as TiO_2 nanotubes,[7] SiO_2 nanoparticles,[11] ZrO_2 nanostructures,[12] zeolites,[9] and graphene oxide (GO)[8,13,14] nanosheets are composed with different polymeric backbones. In this regard, the morphology and electrochemical functionality of nanomaterial as well as its compatibility with the organic matrix have significant effects on the performance of hydroxide conductors.

Over the past few years, GO nanosheets, composed of oxygenated carbons, have demonstrated outstanding physicochemical stability and electrochemical properties.[15−21] Due to the existence of assorted oxygen-containing groups on the GO surface, its properties can be adjusted for specific applications.[8,19,22−24] Concerning nanocomposites, hydrophilic GO nanosheets are easily dispersible in a variety of solvents, which can significantly enhance the interfacial interaction with the polymeric matrix.[15,18,25,26] Formerly, in an investigation by authors[8] it was perceived that GO nanosheets were capable to be functionalized with stable proton-conductive groups and composed with perfluorosulfonic acid (PFSA) polymer, known as Nafion, which significantly increased the proton conductivity and performance by 4 times under the harsh operating conditions of polymer

* Address correspondence to zhwchen@uwaterloo.ca.

Received for review December 14, 2014 and accepted February 2, 2015.

Published online February 02, 2015
10.1021/nn507113c

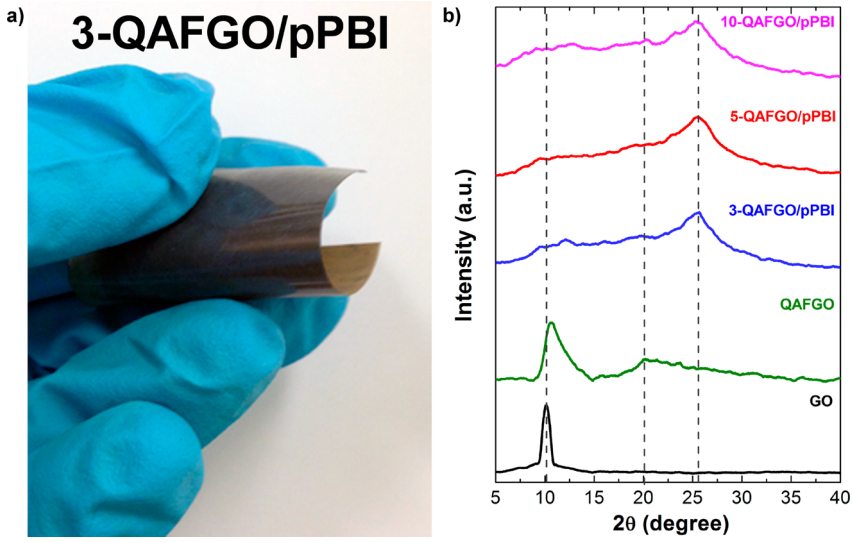

Figure 1. (a) Image of 3-QAFGO/pPBI membrane. (b) XRD patterns of GO, QAFGO, and x-QAFGO/pPBI membranes.

electrolyte fuel cells (*e.g.*, high temperature and low relative humidity).

In this work, for the first time, GO nanosheets were successfully functionalized with stable hydroxide-conductive groups. Dimethyloctadecyl [3-(trimethoxysilyl)-propyl]ammonium chloride (DMAOP) was selected as the precursor, which is an organoalkoxysilane having quaternary ammonium (QA) groups with a linear formula of $[(CH_3O)_3Si(CH_2)_3N(CH_3)_2(CH_2)_{17}CH_3]Cl$. The hydroxide conductivity and the alkaline stability in the highly surface-active DMAOP is provided by quaternary ammonium groups and bulky hydrocarbon chains ($(CH_2)_{17}CH_3$) attached to ammonium cations, respectively.[27,28] The functionalization of GO nanosheets with QA-contained DMAOP (QAFGO) was accomplished through the coupling of trimethoxysilyl group ($(CH_3O)_3Si$) in DMAOP with oxygenated functional groups on GO. According to another study performed by the authors,[6] porous polybenzimidazole (pPBI) was selected as the polymeric backbone for the QAFGO nanocomposite membrane, which provides higher surface area and efficient open paths for hydroxides to be transferred. The high surface area of pPBI enables the exfoliated QAFGO nanosheets to pass through the macropores and have effective interactions with the polymeric matrix. Different loadings of QAFGOs were composed with 70 wt % pPBI, denoted as *x*-QAFGO/pPBI, in which *x* exhibited the weight percentage of QAFGO in the nanocomposite membrane. The morphology, elemental structure, thermo-physicochemical stability, and electrochemical properties of QAFGO and *x*-QAFGO/pPBI membranes were thoroughly characterized using different spectroscopic and microscopic methods. To assess the functionality of QAFGO/pPBI nanocomposite in an alkaline electrochemical system, it was assembled in an alkaline fuel cell (AFC) setup and then compared to commercial Fumapem FAA membrane from FuMA-Tech GmbH. The fabricated nanocomposite QAFGO/pPBI membranes exhibited outstanding hydroxide-conductivity, physicochemical stability, and high AFC performance. Considering the remarkable accomplishments in this discovery, QAFGO nanocomposites demonstrate promising potential to be employed as a reliable hydroxide conductor for electrochemical devices working in harsh alkaline media.

RESULTS AND DISCUSSION

The image of a flexible 3-QAFGO/pPBI nanocomposite membrane in Figure 1a shows the uniform distribution of QAFGO into the pPBI structure. Likewise, in all *x*-QAFGO/pPBI membranes, the QAFGO was uniformly dispersed and incorporated into the pPBI backbone. In order to determine how QAFGO nanosheets were exfoliated and dispersed in pPBI, the XRD of GO, QAFGO, and *x*-QAFGO/pPBI membranes were studied in Figure 1b. The sharp and narrow diffraction-peak of GO appeared at $2\theta = 10.15°$ exhibited a *d*-spacing of 8.7 Å.[29,30] When GO was functionalized with bulky QA groups, a much broader peak was observed at $2\theta = 10.70°$ and $2\theta = 20°$. This indicated that DMAOP was successfully bonded to GO, which expanded the distance of the nanosheets and generated defects on GO surface. The new broad peak $2\theta = 20°$ in QAFGO also revealed that the functionalized nanosheets had less tendency toward stacking and more free layers of QAFGO were produced.[31] After different loadings of QAFGO were incorporated into the matrix of pPBI, the XRD patterns of *x*-QAFGO/pPBI membranes displayed same diffraction peaks at about $2\theta = 25.5°$. The highly broad peak of *x*-QAFGO/pPBIs disclosed their amorphous structure. Moreover, the disappearance of the characteristic diffraction-peak of GO plainly explained the complete exfoliation and uniform distribution of QAFGO into pPBI backbone.[13,14] Specifically, when

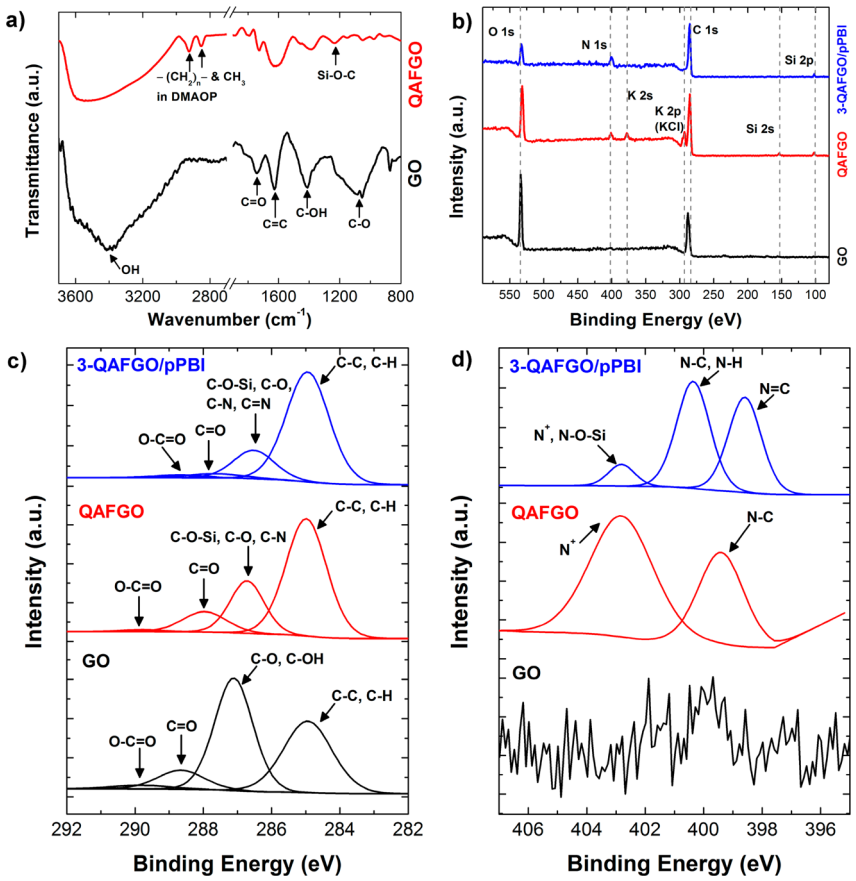

Figure 2. (a) FT-IR spectra, (b) wide region XPS spectra, (c) deconvoluted XPS spectra in the C 1s region, and (d) deconvoluted XPS spectra in the N 1s region of GO, QAFGO, and 3-QAFGO/pPBI membrane.

QAFGO nanosheets were blended with pPBI polymer and casted to form the nanocomposite membrane, QAFGO layers were separated and the polymer chains diffused between the exfoliated nanosheets. This can also be seen in the cross-sectional SEM images in Figure 4.

To confirm the successful alkaline functionalization of GO, FT-IR spectra of GO and QAFGO were compared in Figure 2a. In the GO spectrum, the assigned peaks to epoxy (C—O), carbon—hydroxyl (C—OH), sp2 carbon (C═C), carbonyl (C═O), and free hydroxyl (OH) at 1053.96, 1411.74, 1627.71, 1741.49, and 3416.45 cm^{-1} were in agreement with the literature, respectively.[8,13,32−34] In QAFGO spectrum, it was observed that the broad peak of epoxy at 1053.96 cm^{-1} in GO disappeared and alternatively, a new small peak emerged at 1233.32 cm^{-1} attributing to carbon-siloxane (C—O—Si) bond.[35,36] This revealed that epoxy groups are clearly capable to react with trimethoxysilyl in DMAOP. In addition, the two small peaks appearing at 2852.34 and 2924.66 cm^{-1} are due to methyl and long chains of methylene groups in DMAOP,[35,36] supporting the effective reaction between DMAOP and GO.

To approve the FT-IR results, the XPS analysis was carried out to thoroughly study the interactions between DMAOP and GO as well as QAFGO and pPBI. In the wide-range XPS patterns displayed in Figure 2b, two new peaks other than C 1s and O 1s were observed for QAFGO and 3-QAFGO/pPBI at binding energies of 102.08 and 401.08 eV, attributed to Si 2p and N 1s components, respectively. This confirmed the successful coupling of QA-containing precursor (DMAOP) onto the surface of the GO nanosheets and QAFGO with pPBI. Comprehensive chemical-bonding analysis was carried out through deconvoluted XPS of C 1s (Figure 2c) and N 1s (Figure 2d) for GO, QAFGO, and 3-QAFGO/pPBI. The exhibited C 1s spectra of GO were in compliance with many authorized references.[8,13,32,33,35,37−41] According to C 1s spectra of QAFGO and 3-QAFGO/pPBI in Figure 2c, the peaks of oxygenated carbon groups in GO have shifted to lower binding energies, indicating a change in the degree of surface oxidation after DMAOP functionalization and pPBI composition. Compared to GO, it was seen that the peak intensity at 286.68 eV was significantly decreased in QAFGO and 3-QAFGO/pPBI composite, assigned to the higher reactivity of epoxy groups with trimethoxysilyl in DMAOP which is in accord with FT-IR results. In addition to carbon-siloxane bonds, the broad peak at 286.68 eV represents the carbon—ammonium in DMAOP and carbon—nitrogen peaks in 3-QAFGO/pPBI. Furthermore, the peak intensity increase of C—C/C—H

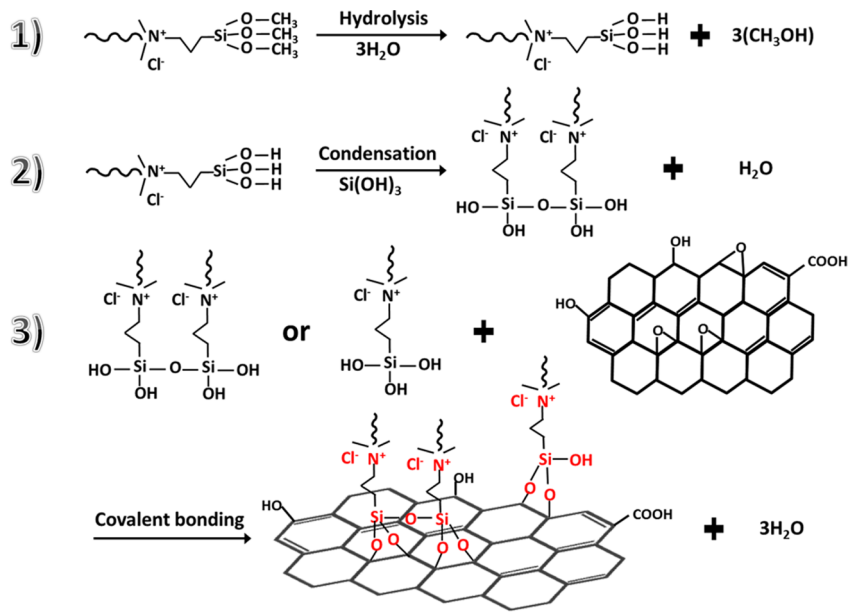

Figure 3. Proposed three-step reaction mechanism for GO surface functionalization with DMAOP.

bonds at 284.98 eV evidently demonstrated the existence of octadecyl and propyl chains coming from DMAOP in QAFGO as well as sp2 and sp3 hybrid orbitals in pPBI.[13,32,33,35,39−41] To further analyze the type of carbon−nitrogen bonds, the N 1s spectra of QAFGO and 3-QAFGO/pPBI in Figure 2d were studied. The displayed peaks at 399.38 and 402.88 eV were assigned to quaternary ammonium and ammonium cations in QAFGO, respectively. When composed with pPBI, the pyridinic N═C and pyrrolic N−C/N−H bonds appeared at 398.58 and 400.38 eV, respectively, due to the existence of imidazole groups. At a higher bond energy of 402.78 eV, a small broad peak was seen which could be attributed to both ammonium cation in QAFGO and pyridinic nitrogen−siloxane bond in 3-QAFGO/pPBI.[32,42−44] The latter might signify that some of the existent siloxane groups in QAFGO were bonded to pyridinic nitrogen of imidazole in pPBI. Such interactions can increase the chemical stability of *x*-QAFGO/pPBI composite membranes to a greater extent.

On the basis of the achieved outcomes from the elemental analysis and reviewed literature,[45,46] the possible reaction mechanism for the surface functionalization of GO nanosheets with DMAOP is illustrated in Figure 3. DMAOP group as the functional precursor is composed of one organofunctional group, $[N^{+}(CH_3)_2(CH_2)_{17}CH_3]Cl^{-}$, and three hydrolyzable trimethoxysilyls, $Si(CH_3O)_3$. First, the trimethoxy groups (*i.e.*, $(CH_3O)_3$) of trimethoxysilyl are hydrolyzed to form silanols, $Si(OH)_3$. The required water for hydrolysis can come from GO surface and the atmosphere. Second, the produced silanols may be condensed to form silanol oligomers. Then, in the last step the free silanols or their oligomers are covalently bonded with oxygenated groups of GO by losing water. Among different oxygenated groups of GO, epoxy groups are predominantly reactive with DMAOP, confirmed by XPS and FT-IR results. Subsequently, the unbonded organofunctional group, *i.e.*, dimethyloctadecylammonium chloride, is accessible for hydroxide exchange.

To investigate the morphology and elemental distribution, the cross-sectional SEM images and oxygen EDX mapping of *x*-QAFGO/pPBI membranes are exhibited in Figure 4. In parts a, d, and g of Figure 4, the low-resolution cross-sectional images of *x*-QAFGO/pPBIs are shown (*x* = 3, 5, and 10, respectively). Parts b, e, and h of Figure 4 exhibit the high-resolution SEM images in which by increasing the loading of QAFGO, *i.e.*, 3−10 wt %, more exfoliated layers of QAFGO could be seen on the porous PBI. Parts c, f, and i of Figure 4 illustrate the oxygen EDX mappings of *x*-QAFGO/pPBI samples which were taken after 20 frames with an exposed time of 30 s for each. The increase of QAFGO composition has resulted in more dense oxygen distribution on porous PBI, specifying more available ion-conductive sites in 10-QAFGO/pPBI.

TGA was utilized to probe the influence of QAFGO on the thermal stability of composite pPBI membranes under nitrogen. The results are displayed in Figure 5a. Before the tests were run, the samples were maintained at room temperature and 30% RH in a humidity chamber for 1 h. Compared to GO, the QAFGO exhibited remarkably higher thermal stability. The notable GO weight loss of 50% from 150 to 250 °C was attributed to the decomposition of the oxygen-containing functional groups.[47,48] Through the alkalization of GO with bulky organosiloxane precursor, the thermal stability of functional groups significantly increased from 150 to 700 °C with a weight loss of 38%. The weight loss before 150 °C was assigned to the removal

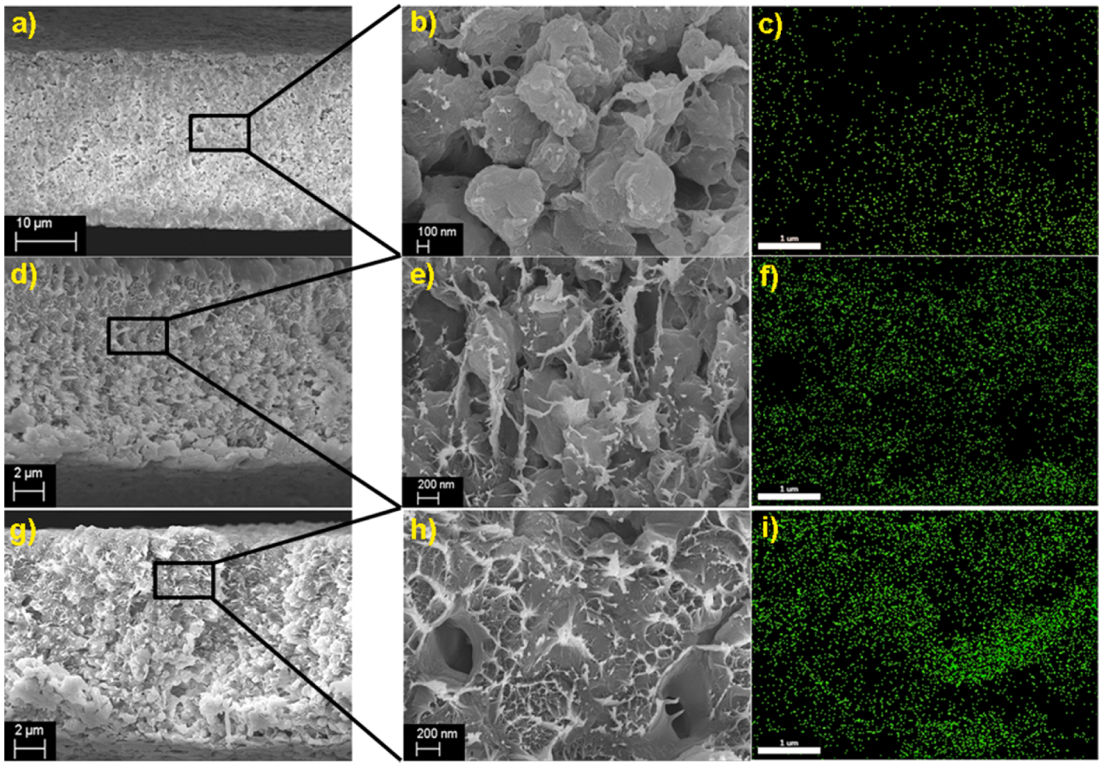

Figure 4. Low-resolution cross-sectional images from SEM of (a) 3-QAFGO/pPBI, (d) 5-QAFGO/pPBI, and (g) 10-QAFGO-pPBI membranes. High-resolution cross-sectional images from SEM of (b) 3-QAFGO/pPBI, (e) 5-QAFGO/pPBI, and (h) 10-QAFGO-pPBI membranes. EDX mapping of oxygen element in (c) 3-QAFGO/pPBI, (f) 5-QAFGO/pPBI, and (i) 10-QAFGO-pPBIs.

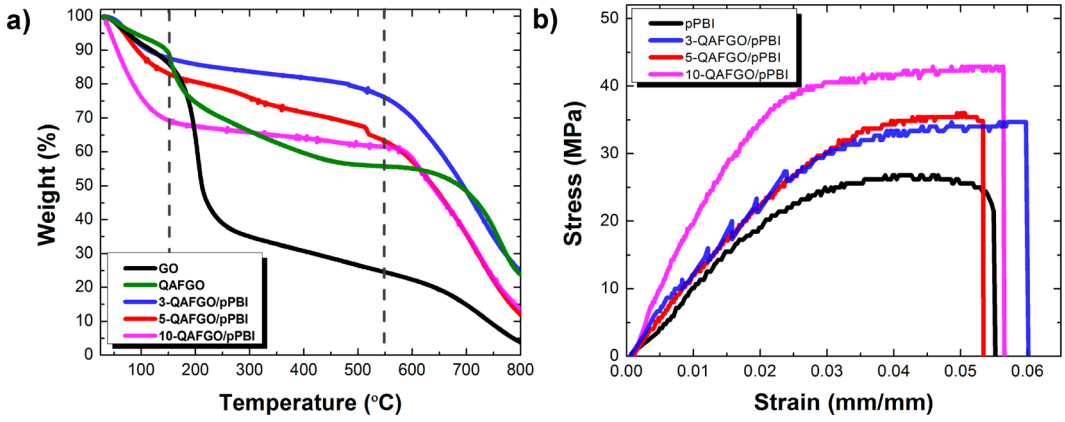

Figure 5. (a) TGA curves of GO, QAFGO, and *x*-QAFGO/pPBI membranes under nitrogen with 10 °C min^{-1} heating rate. (b) Stress−strain plot of pPBI and *x*-QAFGO/pPBI membranes at room temperature (23 °C) and relative humidity (35%).

of unvaporized bound-water molecules, absorbed by all samples. It was seen that the increase of QAFGO loading in composite pPBIs has substantially improved the water retention since the water weight loss of 10-QAFGO/pPBI and 3-QAFGO/pPBI was approximately 30% and 12%, respectively. Considering the decomposition temperature of nanocomposite pPBI membranes, 3-QAFGO/pPBI and 5-QAFGO/pPBI started to degrade at about 550 °C, whereas 10-QAFGO/pPBI decomposition temperature was shifted to 600 °C. TGA results revealed the high potential of 10-QAFGO/pPBI as a stable and water-retentive hydroxide conductor for systems working at elevated temperatures.

To study the effect of QAFGO loadings on the mechanical strength of porous PBI, the tensile test was performed. The typical stress−strain curves for pPBI and *x*-QAFGO/pPBI membranes are displayed in Figure 5b. The tensile strength, Young's modulus, elongation at break, and toughness are listed in Table 1. According to the previous study, the pPBI showed a nonlinear trend, assigned to the plasticity caused by its porous structure.[6] It was seen that the increase of QAFGO amount lessened the nonlinear behavior of stress−strain curves and plasticity which reinforced the mechanical strength of the composite membrane. According to Figure 5b and Table 1, the tensile

strength and Young's modulus increased from 26.79 MPa and 1.04 GPa in pPBI to 42.86 MPa and 2.12 GPa in 10-QAFGO/pPBI, respectively. Moreover, the toughness of 10-QAFGO/pPBI was significantly boosted by 76.41% compared to pPBI. However, the elongation at break did not follow any ascending or descending trend with the addition of QAFGO. 5-QAFGO/pPBI demonstrated the lowest elongation of 5.34%, while 10-QAFGO/pPBI had the highest elongation of 6.01%.

Figure 6a represents the water uptake and cross-wise swelling ratio of all *x*-QAFGO/pPBI membranes. In order to calculate the water uptake and swelling ratio of *x*-QAFGO/pPBI nanocomposite membranes, the samples were immersed in DDI water at room temperature for 48 h. After water was removed from the surface, the weight and thickness of membranes were immediately measured. Then, they were dried in a vacuum oven at 60 °C until a constant weight and thickness were achieved. Finally, the water uptake (WU) and crosswise swelling ratio (C-SWR) were calculated by following equations

$$\text{WU}\ (\%) = \frac{W_w - W_d}{W_d} \times 100 \quad (1)$$

$$\text{C-SWR}\ (\%) = \frac{t_w - t_d}{t_d} \times 100 \quad (2)$$

where W_w and t_w are the weight and thickness of hydrated *x*-QAFGO/pPBI nanocomposites and W_d and t_d are the weight and thickness of dried films.

The results showed that increasing the loading of QAFGO to 3 and 5 wt % resulted in less water uptake compared to bare porous PBI. This could be due to the blockage of pores by QAFGO resulting in smaller water uptake due to less available ion-exchange sites. When the QAFGO composition was increased to 10 wt % higher water uptake of 63.79% was achieved, indicating that higher loading of QAFGO enabled more accessible ion-exchange areas, and thus, a higher amount of water could be absorbed by the composite membrane. Among the nanocomposite membranes the highest C-SWR of 11.46% was gained for 10-QAFGO/pPBI, which was less than that of 13.33% for bare pPBI and higher than that of 3.51% and 9.7% for

TABLE 1. Mechanical Properties of *x*-QAFGO/pPBI Membranes

sample	tensile strength (MPa)	Young's modulus (GPa)	elongation at break (%)	toughness (MPa)
pPBI	26.79	1.04	5.53	1.06
3-QAFGO/pPBI	42.86	2.12	5.66	1.29
5-QAFGO/pPBI	36	1.24	5.34	1.50
10-QAFGO/pPBI	34.67	1.45	6.01	1.87

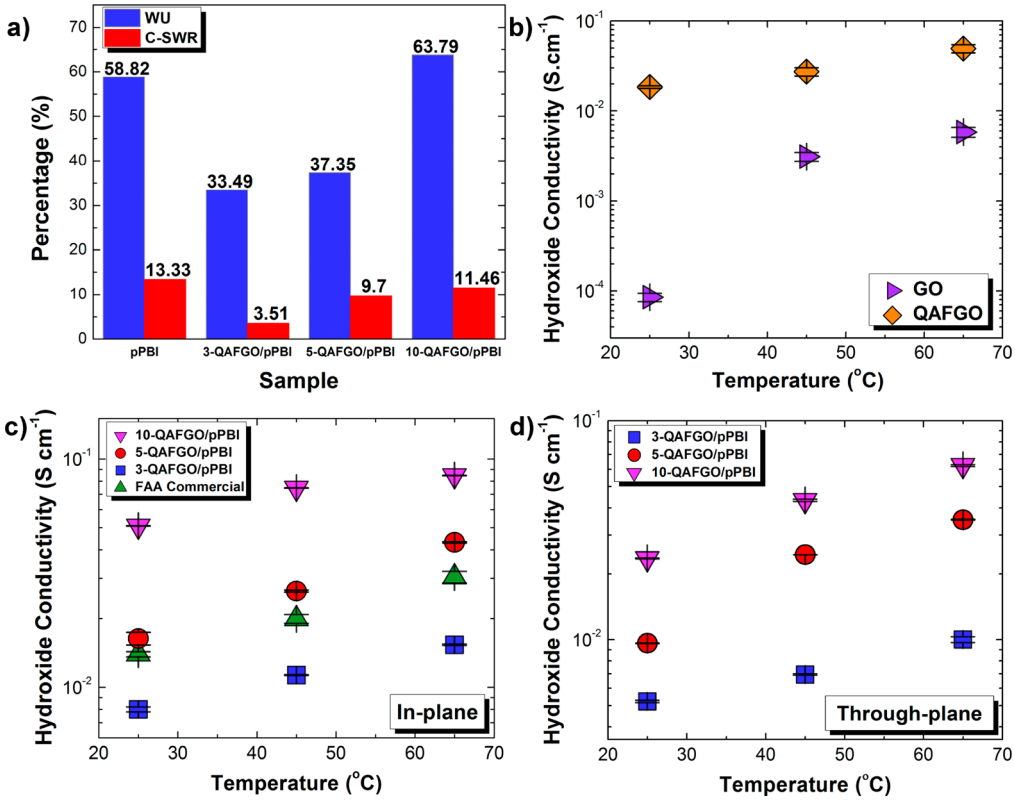

Figure 6. (a) Water uptake and cross-wise swelling ratio of bare pPBI and *x*-QAFGO/pPBI composites. (b) Hydroxide conductivity of GO and QAFGO nanosheets. The hydroxide conductivity of *x*-QAFGO/pPBI membranes compared to the commercial FAA at different temperatures and hydrous conditions in (c) in-plane and (d) through-plane directions.

3-QAFGO/pPBI and 5-QAFGO/pPBI, respectively. This demonstrated that the addition of QAFGO nanofiller has enhanced the mechanical properties of porous PBI by decreasing the membranes swelling.

Parts b, c, and d of Figure 6 illustrate the through-plane and in-plane hydroxide conductivities of GO, QAFGO, and *x*-QAFGO/pPBI membranes under hydrous conditions and different temperatures. The through-plane hydroxide conductivity of GO and QAFGO was measured using a two-electrode electrochemical setup designed for powders at different temperatures.[7,49] First, each of the powdered samples was individually inserted into the middle of a tube cell with a diameter of 1 mm. Then, the samples were pressed between two rod-shaped electrodes for several hours. To gain 100% water saturation, the setup was disassembled from the top and 15 mL of DDI water was injected with a syringe onto the samples. The water was allowed to soak into the samples for 1 h. Then the top electrodes were replaced and the fixture was retorqued. For in-plane direction measurements in nanocomposites, *x*-QAFGO/pPBI membranes were sandwiched in a four-probe cell made of platinum wires and Teflon plates. For the through-plane orientation, the membranes were pressed between two copper strips with 1 cm^2 surface area. In order to acquire the ionic resistance at different temperatures and fully hydrated conditions, all testing instruments were placed in a thermocontrolled chamber with DDI water. For all methods, the real impedance of samples was calculated using AC electrochemical impedance spectroscopy (EIS) in Princeton Versastat MC potentiostat. The frequency range was between 1 MHz and 10 Hz with perturbation voltage amplitude of 10 mV. At a given temperature, the measurements were repeated at least four times with 10 min interval. The hydroxide conductivities were then determined using eq 3

$$\sigma = \frac{L}{RA} \tag{3}$$

where σ denotes the hydroxide conductivity, L is either the distance between the reference electrodes in the four-point cell or the thickness of powdered samples in case of two-electrode setup, R the resistance of the membrane, and A the cross-sectional area in case of the in-plane setup and the area of the electrodes in case of the two-electrode cell.

In both through-plane and in-plane directions, the highest hydroxide conductivity accomplished at 65 °C for all membranes, indicating accelerated ion mobility at elevated temperatures. According to Figure 6b, the hydroxide conductivity of GO outstandingly increased after being functionalized with QA groups. At room temperature and 65 °C, the hydroxide conductivity of QAFGO was 25 and 10 times higher than that of GO, respectively. In Figure 6c, the in-plane hydroxide conductivities of *x*-QAFGO/pPBI membranes were compared to the commercial Fumapem FAA from FuMA-Tech GmbH (35−40 μm thickness, resistivity of 0.59 Ω cm^2 at 20 °C, IEC of 1.2 mmol g^{-1}). Among them, 3-QAFGO/pPBI exhibited smaller hydroxide conductivity at all temperatures compared to commercial FAA membrane. However, as the loading of QAFGO increased to 5 and 10 wt % the hydroxide conductivity surpassed FAA. Such behavior was ascribed to more obtainable ion-exchange sites in nanocomposites with greater amounts of QAFGO. The maximum in-plane hydroxide conductivity was 0.085 S cm^{-1} at 65 °C for 10-QAFGO/pPBI, which was 2.8 times higher than that of commercial FAA. In order to assess the hydroxide conductivity across the thickness of membranes, the through-plane conductivity was measured. On the basis of the obtained results in Figure 6d, the degree of anisotropy was measured, determined as the ratio of the in-plane to the through-plane conductivity. On average, for all nanocomposite membranes, small degree of anisotropy of 1.55 was achieved, indicating that the interconnected pores in pPBI and uniform distribution of exfoliated QAFGO nanosheets aided faster ion-transfer through the thickness of composite membranes.

Figure 7a shows the alkaline electrochemical stability of all *x*-QAFGO/pPBIs compared to commercial FAA membrane. In order to evaluate the alkaline electrochemical stability, all *x*-QAFGO/pPBI nanocomposite membranes were held in a boiling solution of 6 M KOH. After certain times, each sample was rinsed and stored in DDI water before remeasuring the hydroxide-conductivity stability. It was seen that the electrochemical stability of FAA was too low such that after 3 h being exposed to boiling 6 M KOH, the membrane dramatically degraded. On the contrary, all *x*-QAFGO/pPBI membranes maintained their in-plane ionic conductivity for 21 days. The reduced conductivity of 3-QAFGO/pPBI, 5-QAFGO/pPBI, and 10-QAFGO/pPBI was 18%, 11.9%, and 10.01%, respectively, indicating that increase of QAFGO loading in the nanocomposite membrane resulted in more stable hydroxide conductivity. The relatively high alkaline-stability results were assigned to the bulky and long hydrocarbon chains attached to water-retentive ammonium groups on QAFGO nanosheets in nanocomposite membranes.

To assess the functionality of QAFGO/pPBI nanocomposite in an alkaline electrochemical system, the membrane was assembled in an AFC setup. In Figure 7b the single AFC performance of 10-QAFGO/pPBI membrane was compared to that of FAA commercial, evaluated in fully humidified H_2/O_2 system at 50 °C. The open circuit voltages (OCVs) were 1.025 and 0.98 V for FAA and 10-QAFGO/pPBI, respectively, demonstrating that both had low hydrogen permeability. The smaller OCV value of 10-QAFGO/pPBI compared to FAA was attributed to the porous nature of

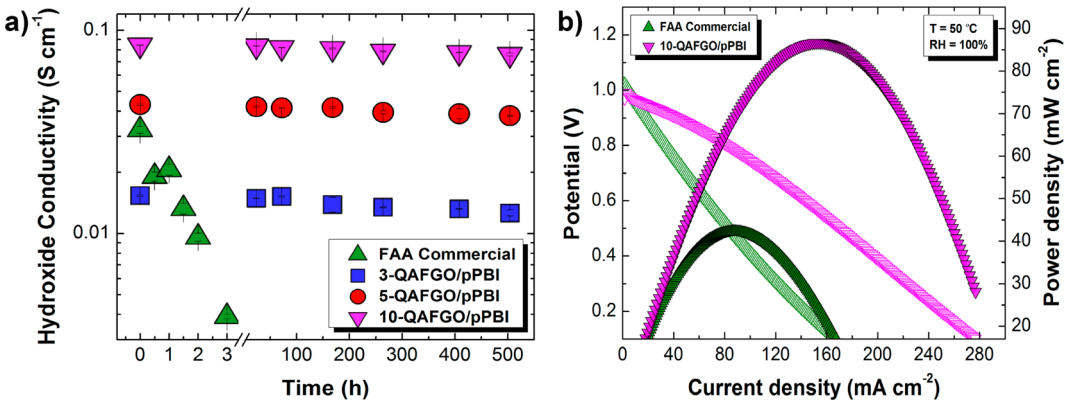

Figure 7. (a) Alkaline electrochemical stability of FAA and *x*-QAFGO/pPBI membranes at 65 °C and hydrous conditions. (b) Single AFC polarization and power density curves employing FAA commercial and 10-QAFGO/pPBI membranes.

10-QAFGO/pPBI nanocomposite in which hydrogen crossover may occur more than that for nonporous commercial FAA. The peak power density of 86.68 mW cm^{-2} for 10-QAFGO/pPBI was about 2 times higher than that of 42.21 mW cm^{-2} for FAA commercial. The better performance was primarily attributed to the excellent hydroxide conductivity and strong water retention properties of the nanocomposite membrane. In 10-QAFGO/pPBI, the existing bulky quaternary ammonium groups on the large surface of exofoliated GO nanosheets provided more facile hopping of hydroxides to enhance the ionic conductivity. Clearly, alkaline-functionalized graphene oxide composed with porous PBI may be a significant potential hydroxide conductor for alkaline-based electrochemical devices due to its high hydroxide conductivity, alkaline-electrochemical stability and thermo-physicochemical stability.

CONCLUSIONS

In this work, for the first time, GO nanosheets were successfully functionalized with hydroxide-conductive groups *via* DMAOP precursor containing bulky quaternary ammonium groups. The fabricated QAFGO was then incorporated into porous PBI to form a hydroxide-conductive and stable nanocomposite membrane. The presence of bulky QA groups interacted with large surface areas of GO and pPBI significantly enhanced the hydroxide conductivity to 0.085 S cm^{-1}, which was stable for 21 days, whereas FAA commercial film degraded just after 3 h. A single AFC setup containing 10-QAFGO/pPBI was assembled to evaluate the effect of the developed nanocomposite on the performance improvement of an electrochemical device working in alkaline medium. High AFC performance with a peak power density of 86.68 mW cm^{-2} was attained when compared to FAA film with that of 42.21 mW cm^{-2}. Apart from high performance, *x*-QAFGO/pPBI membranes also exhibited excellent physicochemical and thermal stability. The achieved results demonstrated that the QAFGO/pPBI nanocomposite has the capability to be a promising and fast hydroxide conductor for various alkaline-electrochemical applications.

EXPERIMENTAL SECTION

Synthesis of GO. In this work, the improved Hummers' method[37] was employed for the synthesis of GO from natural graphite flakes, which is the most commonly used approach at the present time. Graphite powder (2 g) was added to the mixture of 360 mL of concentrated H_2SO_4 and 40 mL of H_3PO_4 in a round-bottom flask. After 30 min of stirring, 18 g of $KMnO_4$ was added slowly as it was a strong oxidizing agent. The temperature of the mixture was increased to 50 °C, and the oxidative reaction of graphite lasted 16 h. Afterward, the solution was cooled, and 400 mL of distilled deionized (DDI) water and then 20 mL of H_2O_2 were added dropwise, and the mixture was stirred for 30 min to remove all impurities. In order to collect the produced GO nanosheets, the final mixture was washed and centrifuged with DDI, HCl, and ethanol, respectively. Finally, the GO was freeze-dried.

Functionalization of QAFGO. In order to alkali-functionalize GO nanosheets (QAFGO) with quaternary ammonium groups the DMAOP precursor was adopted. First, 0.1 g of GO fluffy powder was dispersed and exfoliated in 50 mL of toluene by 2 h sonication to obtain a stable GO suspension. After addition of 10 g of DMAOP to GO, the reaction was carried out at room temperature for 2 days. Then, the product was centrifuged and washed several times with ethanol to remove the toluene and unreacted traces of DMAOP. The chlorine (Cl^-) counterion in obtained QAFGO was exchanged with hydroxide (OH^-) by adding 1 M KOH to it overnight. Finally, the product was washed and centrifuged several times with DDI water and then freeze dried.

Synthesis of PBI. The detailed synthesis of PBI has been explained in the previous work.[6] In summary, 4.7 mmol of 3,3′-diaminobenzidine (DAB, Aldrich) with an equivalent molar amount of isophthalic acid (IPA, Aldrich) were dissolved into polyphosphoric acid (PPA, Alfa Aesar), and the mixture was reacted for 7 h at 200 °C. The dark reddish brown and viscous product was quenched by pouring it into a large amount of cold water. The formed PBI fibers were stirred and washed for 48 h in DDI water and subsequently for 7 h in 2 M KOH solution followed by drying in an oven at 100 °C overnight. The average molecular weight of 104167 ± 1.898 g·mol^{-1} was evaluated for PBI by using static light scattering method and measuring the inverse of the intercept of the linear interpolation in the resulted Zimm plot.

Casting *x*-QAFGO/pPBI Membranes. *x*-QAFGO/pPBI nanocomposite membranes were casted by mixing *x* (= 3, 5, or 10) wt %

QAFGO with an appropriate amount of PBI dissolved in DMSO. Dibutyl phthalate (DBP) was added to the QAFGO/PBI mixture to produce 70 wt % porous composite film. The final uniform solution was cast on a glass plate at 60 °C for 2 days and then gradually heat treated from 100 to 190 °C for 4 h in order to fully evaporate the solvent. The obtained nanocomposite membranes were immersed in methanol for 1 h to extract DBP and introduce porosity. On average, the real porosity of nanocomposites was about 67.55%. After drying at 60 °C all *x*-QAFGO/pPBI composites were treated with 6 M KOH for 1 day and finally stored in DDI water for future physicochemical and electrochemical characterization tests.

Preparation AFC Setup. The performance of 10-QAFGO/pPBI, pPBI, and FAA commercial in a fuel cell setup was determined using a single cell membrane electrode assembly (MEA) setup. The anode and cathode catalyst layers were prepared by mixing and ultrasonicating appropriate amounts of Pt/C (45.7 wt % Pt, TKK Corp.), AS-4 ionomer from Tokuyama Corp., and 2-propanol as the solvent. The inks were sprayed on gas diffusion layers (GDL, SIGRACET GDL10 BB) and then dried at room temperature overnight until the desired catalyst loading of 0.3 mg cm^{-2} was achieved for both anode and cathode. The MEA with an active electrode area of 5 cm^2 was obtained by pressing the catalyst-coated GDLs onto the membrane at room temperature with 3 t loading for 3 min. For each sample, the MEA was assembled into the fuel cell hardware (850e Multi-Range Fuel Cell Test System, Scribner Associates) with gas flow rate of 0.2 L min^{-1} and back pressure of 6 psi for both hydrogen and oxygen.

Thermal, Physical, and Chemical Characterization Tests. The elemental and chemical-bonding analyses of QAFGO and *x*-QAFGO/pPBI membranes were determined *via* XPS (Thermo Scientific Al K-Alpha X-ray source) and FT_IR (Avatar 320). The presence and distribution degree of QAFGO inside the porous PBI were shown by XRD (INEL XRG 3000), cross-sectional SEM images, and EDX mapping (LEO FESEM 1530) of all samples. To assess the thermal stability, TGA was performed under nitrogen with a TGAQ500 V20.10 instrument in the temperature range from 25 to 900 °C at the heating rate of 10 °C min^{-1}. The mechanical properties of all membranes were determined by a tension testing machine (ADMET 7603- 5 kN) in ambient atmosphere (23 °C and 35% relative humidity) at a tension speed of 5 mm min^{-1}. The size of the species was 5 mm wide, 35 mm long, and 35 μm thick.

Conflict of Interest: The authors declare no competing financial interest.

Acknowledgment. This work was financially supported by the Natural Sciences and Engineering Research Council of Canada (NSERC) and the University of Waterloo.

REFERENCES AND NOTES

1. Kreuer, K.-D. Ion Conducting Membranes for Fuel Cells and Other Electrochemical Devices. *Chem. Mater.* **2013**, *26*, 361–380.
2. Wang, Y.-J.; Qiao, J.; Baker, R.; Zhang, J. Alkaline Polymer Electrolyte Membranes for Fuel Cell Applications. *Chem. Soc. Rev.* **2013**, *42*, 5768–5787.
3. Zarrin, H.; Wu, J.; Fowler, M.; Chen, Z. High Durable Pek-Based Anion Exchange Membrane for Elevated Temperature Alkaline Fuel Cells. *J. Membr. Sci.* **2012**, *394—395*, 193–201.
4. Kim, D. S.; Labouriau, A.; Guiver, M. D.; Kim, Y. S. Guanidinium-Functionalized Anion Exchange Polymer Electrolytes via Activated Fluorophenyl-Amine Reaction. *Chem. Mater.* **2011**, *23*, 3795–3797.
5. Fu, J.; Qiao, J.; Lv, H.; Ma, J.; Yuan, X.-Z.; Wang, H. Alkali Doped Poly (Vinyl Alcohol)(Pva) for Anion-Exchange Membrane Fuel Cells: Ionic Conductivity, Chemical Stability and Ft-Ir Characterizations. *ECS Trans.* **2010**, *25*, 15–23.
6. Zarrin, H.; Jiang, G.; Lam, G. Y.-Y.; Fowler, M.; Chen, Z. High Performance Porous Polybenzimidazole Membrane for Alkaline Fuel Cells. *Int. J. Hydrogen Energy* **2014**, *39*, 18405–18415.
7. Jun, Y.; Zarrin, H.; Fowler, M.; Chen, Z. Functionalized Titania Nanotube Composite Membranes for High Temperature Proton Exchange Membrane Fuel Cells. *Int. J. Hydrogen Energy* **2011**, *36*, 6073–6081.
8. Zarrin, H.; Higgins, D.; Yu, J.; Fowler, M.; Chen, Z. Functionalized Graphene Oxide Nanocomposite Membrane for Low Humidity and High Temperature Proton Exchange Membrane Fuel Cells. *J. Phys. Chem. C* **2011**, *115*, 20774–20781.
9. Chen, Z.; Holmberg, B.; Li, W.; Wang, X.; Deng, W.; Munoz, R.; Yan, Y. Nafion/Zeolite Nanocomposite Membrane by in Situ Crystallization for a Direct Methanol Fuel Cell. *Chem. Mater.* **2006**, *18*, 5669–5675.
10. Qu, C.; Zhang, H.; Zhang, F.; Liu, B. A High-Performance Anion Exchange Membrane Based on Bi-Guanidinium Bridged Polysilsesquioxane for Alkaline Fuel Cell Application. *J. Mater. Chem.* **2012**, *22*, 8203–8207.
11. Wu, Y.; Wu, C.; Li, Y.; Xu, T.; Fu, Y. Pva-Silica Anion-Exchange Hybrid Membranes Prepared through a Copolymer Cross-linking Agent. *J. Membr. Sci.* **2010**, *350*, 322–332.
12. Li, X.; Yu, Y.; Meng, Y. Novel Quaternized Poly (Arylene Ether Sulfone)/Nano-Zro2 Composite Anion Exchange Membranes for Alkaline Fuel Cells. *ACS Appl. Mater. Interfaces* **2013**, *5*, 1414–1422.
13. Wang, Y.; Shi, Z.; Fang, J.; Xu, H.; Yin, J. Graphene Oxide/Polybenzimidazole Composites Fabricated by a Solvent-Exchange Method. *Carbon* **2011**, *49*, 1199–1207.
14. Xu, C.; Cao, Y.; Kumar, R.; Wu, X.; Wang, X.; Scott, K. A Polybenzimidazole/Sulfonated Graphite Oxide Composite Membrane for High Temperature Polymer Electrolyte Membrane Fuel Cells. *J. Mater. Chem.* **2011**, *21*, 11359–11364.
15. Kulkarni, D.; Choi, I.; Singamaneni, S.; Tsukruk, V. Graphene Oxide-Polyelectrolyte Nanomembranes. *ACS Nano* **2010**, *4*, 4667–4676.
16. Wilson, N.; Pandey, P.; Beanland, R.; Young, R.; Kinloch, I.; Gong, L.; Liu, Z.; Suenaga, K.; Rourke, J.; York, S. Graphene Oxide: Structural Analysis and Application as a Highly Transparent Support for Electron Microscopy. *ACS Nano* **2009**, *3*, 2547–2556.
17. Kim, F.; Cote, L.; Huang, J. Graphene Oxide: Surface Activity and Two-Dimensional Assembly. *Adv. Mater.* *22*, 1954—1958.
18. Stankovich, S.; Dikin, D.; Dommett, G.; Kohlhaas, K.; Zimney, E.; Stach, E.; Piner, R.; Nguyen, S.; Ruoff, R. Graphene-Based Composite Materials. *Nature* **2006**, *442*, 282–286.
19. Gao, W.; Wu, G.; Janicke, M. T.; Cullen, D. A.; Mukundan, R.; Baldwin, J. K.; Brosha, E. L.; Galande, C.; Ajayan, P. M.; More, K. L. Ozonated Graphene Oxide Film as a Proton-Exchange Membrane. *Angew. Chem., Int. Ed.* **2014**, *53*, 3588–3593.
20. Wang, H.; Maiyalagan, T.; Wang, X. Review on Recent Progress in Nitrogen-Doped Graphene: Synthesis, Characterization, and Its Potential Applications. *ACS Catal.* **2012**, *2*, 781–794.
21. Yu, S.; Li, N.; Higgins, D.; Li, D.; Li, Q.; Xu, H.; Spendelow, J.; Wu, G. Self-Assembled Reduced Graphene Oxide/Polyacrylamide Conductive Composite Films. *ACS Appl. Mater. Interfaces* **2014**, *6*, 19783–19790.
22. Karim, M. R.; Hatakeyama, K.; Matsui, T.; Takehira, H.; Taniguchi, T.; Koinuma, M.; Matsumoto, Y.; Akutagawa, T.; Nakamura, T.; Noro, S.-i. Graphene Oxide Nanosheet with High Proton Conductivity. *J. Am. Chem. Soc.* **2013**, *135*, 8097–8100.
23. Scott, K. Freestanding Sulfonated Graphene Oxide Paper: A New Polymer Electrolyte for Polymer Electrolyte Fuel Cells. *Chem. Commun.* **2012**, *48*, 5584–5586.
24. Zhang, L. L.; Zhao, X.; Stoller, M. D.; Zhu, Y.; Ji, H.; Murali, S.; Wu, Y.; Perales, S.; Clevenger, B.; Ruoff, R. S. Highly Conductive and Porous Activated Reduced Graphene Oxide Films for High-Power Supercapacitors. *Nano Lett.* **2012**, *12*, 1806–1812.
25. Fang, M.; Wang, K.; Lu, H.; Yang, Y.; Nutt, S. Covalent Polymer Functionalization of Graphene Nanosheets and Mechanical Properties of Composites. *J. Mater. Chem.* **2009**, *19*, 7098–7105.
26. Niyogi, S.; Bekyarova, E.; Itkis, M. E.; McWilliams, J. L.; Hamon, M. A.; Haddon, R. C. Solution Properties of

Graphite and Graphene. *J. Am. Chem. Soc.* **2006**, *128*, 7720–7721.
27. Szczepanowicz, K.; Para, G.; Bouzga, A. M.; Simon, C.; Yang, J.; Warszynski, P. Hydrolysis of Silica Sources: Aps and Dtsacl in Microencapsulation Processes. *Fizykochem. Probl. Mineralurgii* **2012**, *48*, 403–412.
28. Walcarius, A.; Ganesan, V. Ion-Exchange Properties and Electrochemical Characterization of Quaternary Ammonium-Functionalized Silica Microspheres Obtained by the Surfactant Template Route. *Langmuir* **2006**, *22*, 469–477.
29. Li, Z.; Lu, C.; Xia, Z.; Zhou, Y.; Luo, Z. X-Ray Diffraction Patterns of Graphite and Turbostratic Carbon. *Carbon* **2007**, *45*, 1686–1695.
30. Jeong, H.-K.; Lee, Y. P.; Lahaye, R. J.; Park, M.-H.; An, K. H.; Kim, I. J.; Yang, C.-W.; Park, C. Y.; Ruoff, R. S.; Lee, Y. H. Evidence of Graphitic Ab Stacking Order of Graphite Oxides. *J. Am. Chem. Soc.* **2008**, *130*, 1362–1366.
31. He, H.; Gao, C. General Approach to Individually Dispersed, Highly Soluble, and Conductive Graphene Nanosheets Functionalized by Nitrene Chemistry. *Chem. Mater.* **2010**, *22*, 5054–5064.
32. Compton, O. C.; Dikin, D. A.; Putz, K. W.; Brinson, L. C.; Nguyen, S. T. Electrically Conductive "Alkylated" Graphene Paper via Chemical Reduction of Amine-Functionalized Graphene Oxide Paper. *Adv. Mater.* **2010**, *22*, 892–896.
33. Park, S.; Dikin, D.; Nguyen, S.; Ruoff, R. Graphene Oxide Sheets Chemically Cross-Linked by Polyallylamine. *J. Phys. Chem. C* **2009**, *113*, 15801–15804.
34. Wan, W.; Zhao, Z.; Hu, H.; Gogotsi, Y.; Qiu, J. Highly Controllable and Green Reduction of Graphene Oxide to Flexible Graphene Film with High Strength. *MRS Bull.* **2013**, *48*, 4797–4803.
35. Tang, X.-Z.; Li, W.; Yu, Z.-Z.; Rafiee, M. A.; Rafiee, J.; Yavari, F.; Koratkar, N. Enhanced Thermal Stability in Graphene Oxide Covalently Functionalized with 2-Amino-4, 6-Didodecylamino-1, 3, 5-Triazine. *Carbon* **2011**, *49*, 1258–1265.
36. Smith, A. L. Infrared Spectra-Structure Correlations for Organosilicon Compounds. *Spectrochim. Acta* **1960**, *16*, 87–105.
37. Marcano, D. C.; Kosynkin, D. V.; Berlin, J. M.; Sinitskii, A.; Sun, Z.; Slesarev, A.; Alemany, L. B.; Lu, W.; Tour, J. M. Improved Synthesis of Graphene Oxide. *ACS Nano* **2010**, *4*, 4806–4814.
38. Wang, S. J.; Geng, Y.; Zheng, Q.; Kim, J.-K. Fabrication of Highly Conducting and Transparent Graphene Films. *Carbon* **2010**, *48*, 1815–1823.
39. Wang, H.; Hao, Q.; Yang, X.; Lu, L.; Wang, X. Effect of Graphene Oxide on the Properties of Its Composite with Polyaniline. *ACS Appl. Mater. Interfaces* **2010**, *2*, 821–828.
40. Xue, Y.; Liu, Y.; Lu, F.; Qu, J.; Chen, H.; Dai, L. Functionalization of Graphene Oxide with Polyhedral Oligomeric Silsesquioxane (Poss) for Multifunctional Applications. *J. Phys. Chem. Lett.* **2012**, *3*, 1607–1612.
41. Haubner, K.; Murawski, J.; Olk, P.; Eng, L. M.; Ziegler, C.; Adolphi, B.; Jaehne, E. The Route to Functional Graphene Oxide. *ChemPhysChem* **2010**, *11*, 2131–2139.
42. Yang, W. J.; Neoh, K.-G.; Kang, E.-T.; Teo, S. L.-M.; Rittschof, D. Stainless Steel Surfaces with Thiol-Terminated Hyperbranched Polymers for Functionalization *via* Thiol-Based Chemistry. *Polym. Chem.* **2013**, *4*, 3105–3115.
43. Liu, G.; Li, X.; Lee, J.-W.; Popov, B. N. A Review of the Development of Nitrogen-Modified Carbon-Based Catalysts for Oxygen Reduction at USC. *Catal. Sci. Technol.* **2011**, *1*, 207–217.
44. Yang, X.; Tu, Y.; Li, L.; Shang, S.; Tao, X.-m. Well-Dispersed Chitosan/Graphene Oxide Nanocomposites. *ACS Appl. Mater. Interfaces* **2010**, *2*, 1707–1713.
45. Hou, S.; Su, S.; Kasner, M. L.; Shah, P.; Patel, K.; Madarang, C. J. Formation of Highly Stable Dispersions of Silane-Functionalized Reduced Graphene Oxide. *Chem. Phys. Lett.* **2010**, *501*, 68–74.
46. Lakshminarayana, G.; Nogami, M. Inorganic−Organic Hybrid Membranes with Anhydrous Proton Conduction Prepared from Tetramethoxysilane/Methyl-Trimethoxysilane/Trimethylphosphate and 1-Ethyl-3-Methylimidazolium-Bis(Trifluoromethanesulfonyl) Imide for H_2/O_2 Fuel Cells. *Electrochim. Acta* **2010**, *55*, 1160–1168.
47. Zhang, W. L.; Choi, H. J. Silica-Graphene Oxide Hybrid Composite Particles and Their Electroresponsive Characteristics. *Langmuir* **2012**, *28*, 7055–7062.
48. Stankovich, S.; Dikin, D. A.; Piner, R. D.; Kohlhaas, K. A.; Kleinhammes, A.; Jia, Y.; Wu, Y.; Nguyen, S. T.; Ruoff, R. S. Synthesis of Graphene-Based Nanosheets via Chemical Reduction of Exfoliated Graphite Oxide. *Carbon* **2007**, *45*, 1558–1565.
49. Yuan, X.-Z.; Song, C.; Wang, H.; Zhang, J.Electrochemical Impedance Spectroscopy in Pem Fuel Cells.*Fundamentals and Applications*; Springer-Verlag: London, **2010**